Phonon anomalies in some iron telluride materials

C. C. Homes,* Y. M. Dai,† J. Schneeloch, R. D. Zhong, and G. D. Gu

Condensed Matter Physics and Materials Science Department, Brookhaven National Laboratory, Upton, New York 11973, USA

(Received 19 November 2015; revised manuscript received 24 February 2016; published 21 March 2016)

The detailed temperature dependence of the infrared-active mode in $Fe_{1.03}Te$ ($T_N \simeq 68$ K) and $Fe_{1.13}Te$ ($T_N \simeq 56$ K) has been examined, and the position, width, strength, and asymmetry parameter have been determined using an asymmetric Fano profile superimposed on an electronic background. In both materials the frequency of the mode increases as the temperature is reduced; however, there is also a slight asymmetry in the line shape, indicating that the mode is coupled to either spin or charge excitations. Below T_N there is an anomalous decrease in frequency, and the mode shows little temperature dependence, at the same time becoming more symmetric, suggesting a reduction in spin- or electron-phonon coupling. The frequency of the infrared-active mode and the magnitude of the shift below T_N are predicted reasonably well by first-principles calculations; however, the predicted splitting of the mode is not observed. In superconducting $FeTe_{0.55}Se_{0.45}$ ($T_c \simeq 14$ K) the infrared-active E_u mode displays asymmetric line shape at all temperatures, which is most pronounced between 100 and 200 K, indicating the presence of either spin- or electron-phonon coupling, which may be a necessary prerequisite for superconductivity in this class of materials.

DOI: 10.1103/PhysRevB.93.125135

I. INTRODUCTION

The discovery of superconductivity in iron-based materials has prompted a thorough investigation of this class of materials in an effort to understand the mechanism responsible for the superconductivity, as well as the normal state from which it emerges [1]. While much of this work has focused on the electronic and magnetic structure, lattice vibrations are also useful for probing electron-phonon coupling and the effects of chemical substitution [2]. Among iron-based materials, iron telluride is of particular interest because it is thought to be among the most strongly correlated of the iron-chalcogenide materials [3]. At room temperature, the nearly stoichiometric $Fe_{1+\delta}Te$ is a tetragonal, paramagnetic metal that undergoes a first-order structural and magnetic transition to a monoclinic, antiferromagnetic (AFM) metal at $T_N \simeq 68$ K [4–9]. The introduction of excess iron leads to an increase in the resistivity and the suppression of T_N [10,11]. The substitution of Se for Te in $FeTe_{1-x}Se_x$ suppresses the structural and magnetic transition and results in a superconducting phase for a broad range of compositions [12,13], with a maximum critical temperature of $T_c \simeq 14$ K [14–17]. The optical and transport properties of $Fe_{1+\delta}Te$ and $FeTe_{1-x}Se_x$ have been investigated [17–23], and in addition there have been a number of reports on the vibrational properties of these materials; however, only the Raman-active modes have been studied [24–28], leaving the infrared-active modes largely unexplored.

In this work we examine the optical properties of $Fe_{1.03}Te$ ($T_N \simeq 68$ K) and $Fe_{1.13}Te$ ($T_N \simeq 56$ K) above and below T_N, as well as $FeTe_{0.55}Se_{0.45}$ ($T_c \simeq 14$ K), and determine the detailed temperature dependence of the position, width, strength, and asymmetry parameter of the infrared-active mode using an asymmetric (Fano) line shape; in several cases the electronic properties of these materials have been previously discussed by us [19–21]. In both $Fe_{1+\delta}Te$ materials the infrared-active mode displays a slight asymmetry, suggesting either spin- or electron-phonon coupling, and increases in frequency with decreasing temperature, as expected for an anharmonic decay process; below T_N the mode undergoes an anomalous decrease in frequency at T_N, and the asymmetry parameter decreases, indicating reduced coupling. The vibrational frequencies and atomic intensities have been calculated at the center of the Brillouin zone from first-principles methods for both the high-temperature tetragonal phase and the low-temperature monoclinic phase. In the latter case, spin ordering is shown in some cases to alter the character of the mode, resulting in a large predicted frequency shift below T_N. Interestingly, the predicted splitting of the infrared-active E_u mode below T_N is not observed. In $FeTe_{0.55}Se_{0.45}$ the E_u mode displays an asymmetry at all temperatures, which is most pronounced between 100 and 200 K. The asymmetric profile is a signature of either spin- or electron-phonon coupling, which may be a necessary condition for superconductivity in this class of materials.

II. EXPERIMENT

Single crystals of $Fe_{1.03}Te$ and $Fe_{1.13}Te$ with good cleavage planes (001) were grown by a unidirectional solidification process; these crystals undergo structural and magnetic transitions [4–9] at $T_N \simeq 68$ K and $\simeq 56$ K, respectively. Single crystals with a nominal composition of $FeTe_{0.55}Se_{0.45}$ were also grown using a similar process with $T_c \simeq 14$ K and a transition width of $\simeq 1$ K. The reflectance of these materials with the light polarized in the Fe-As (*a*-*b*) planes has been measured over a wide frequency range ($\simeq 2$ meV to over 3 eV) using an *in situ* evaporation technique [29] for a wide range of temperatures. The complex optical properties have been calculated from a Kramers-Kronig analysis of the reflectance [30]. The large-scale structure and temperature dependence of the optical conductivity of some of these materials have been previously discussed [19–21].

*homes@bnl.gov
†ymdai@lanl.gov

III. RESULTS AND DISCUSSION

Lattice vibrations in solids are often described using a Lorentzian oscillator superimposed on a linear (or polynomial) background. The complex dielectric function $\tilde{\epsilon} = \epsilon_1 + i\epsilon_2$ for the Lorentz oscillator is

$$\tilde{\epsilon}(\omega) = \frac{\Omega_0^2}{\omega_0^2 - \omega^2 - i\gamma_0\omega}, \tag{1}$$

where ω_0, γ_0, and Ω_0 are the position, width, and strength of the vibration, respectively. The complex conductivity is $\tilde{\sigma}(\omega) = \sigma_1 + i\sigma_2 = -2\pi i\,\omega[\tilde{\epsilon}(\omega) - \epsilon_\infty]/Z_0$, where ϵ_∞ is a high-frequency contribution to the real part and $Z_0 \simeq 377\ \Omega$ is the impedance of free space, yielding units for the conductivity of $\Omega^{-1}\,\mathrm{cm}^{-1}$. The real part of the optical conductivity for the oscillator may then be written as

$$\sigma_1(\omega) = \frac{2\pi}{Z_0}\left[\frac{\gamma_0\,\omega^2\Omega_0^2}{\left(\omega_0^2 - \omega_2\right)^2 + \gamma_0^2\omega^2}\right]. \tag{2}$$

While this approach accurately describes a symmetric line shape, the coupling of lattice vibrations to either the spin or electronic background may lead to an asymmetric line shape, often referred to as the Fano profile [31]. The Fano line shape is written as $\sigma_1(\omega) = A[(x+q)^2/(1+x^2)]$, where A is a constant, $x = (\omega - \omega_0)/\gamma_0$, and the asymmetry is described by the dimensionless parameter $1/q^2$. A more useful expression,

$$\sigma_1(\omega) = \frac{2\pi}{Z_0}\frac{\Omega_0^2}{\gamma_0}\frac{(q^2 + 4qx - 1)}{q^2(1+4x^2)}, \tag{3}$$

incorporates the oscillator strength; however, this contains no information about $\sigma_2(\omega)$ and does not satisfy the Kramers-Kronig relation. To resolve this issue a phenomenological dielectric function for a Fano-shaped Lorentz oscillator is employed that is Kramers-Kronig consistent [32,33],

$$\tilde{\epsilon}(\omega) = \frac{\Omega_0^2}{\omega_0^2 - \omega^2 - i\gamma_0\omega}\left(1 + i\frac{\omega_q}{\omega}\right)^2 + \left(\frac{\Omega_0\omega_q}{\omega_0\omega}\right)^2, \tag{4}$$

where $1/q = \omega_q/\omega_0$. Unlike the simple Fano profile, a complex conductivity may be calculated which satisfies $\tilde{\sigma}^*(\omega) = \tilde{\sigma}(-\omega)$. The real part of the optical conductivity is then

$$\sigma_1(\omega) = \frac{2\pi}{Z_0}\frac{\Omega_0^2\left[\gamma_0\omega^2 - 2\left(\omega^2\omega_0 - \omega_0^3\right)/q - \gamma_0\omega_0^2/q^2\right]}{\left(\omega^2 - \omega_0^2\right)^2 + \gamma_0^2\omega^2}. \tag{5}$$

In the $1/q^2 \to 0$ limit a symmetric Lorentzian is recovered [Eq. (2)]; however, as $1/q^2$ increases, the line shape becomes increasingly asymmetric. We adopt this latter form for asymmetric line shapes to fit the infrared-active vibrations in $Fe_{1+\delta}Te$ and $FeTe_{0.55}Se_{0.45}$.

A. $Fe_{1+\delta}Te$

1. Vibrational properties

The real part of the optical conductivity of $Fe_{1.03}Te$ in the region of the infrared-active phonon is shown in Fig. 1(a). The rapid increase in the low-frequency conductivity below T_N has been attributed to the closing of the pseudogap below T_N, leading to an increase in the free-carrier concentration [19]. In the room-temperature tetragonal phase, the $P4/nmm$ space group with two formula units per unit cell yields the irreducible vibrational representation [24]

$$\Gamma_{\mathrm{HT}} = A_{1g} + B_{1g} + 2E_g + A_{2u} + E_u.$$

Two infrared-active modes are expected, a doubly degenerate E_u mode active in the planes and an A_{2u} mode active along the c axis. In the low-temperature monoclinic phase, the $P2_1/m$ space group with two formula units per unit cell yields the irreducible vibrational representation [26]

$$\Gamma_{\mathrm{LT}} = 4A_g + 2B_g + A_u + 2B_u,$$

where the A_u mode is infrared active along the c axis and the E_u mode splits into two B_u modes that are active in the a-b plane.

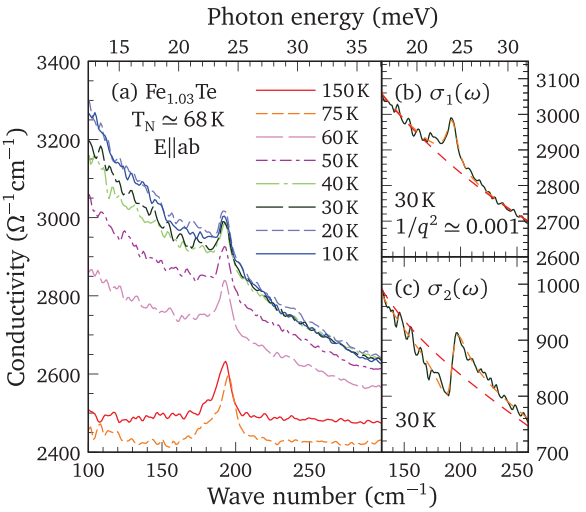

FIG. 1. (a) The real part of the optical conductivity of $Fe_{1.03}Te$ above and below $T_N \simeq 68$ K in the region of the infrared-active mode at $\simeq$196 cm^{-1}. There is no evidence that this mode splits below T_N. (b) Fano oscillator fit (short-dashed line) to $\sigma_1(\omega)$ at 30 K with the Drude-Lorentz background (long-dashed line) and (c) the simultaneous fit to $\sigma_2(\omega)$; note the almost perfectly symmetric profile.

The infrared-active mode is fit simultaneously to the real and imaginary parts of the complex conductivity using the asymmetric line shape described by the dielectric function in Eq. (4) superimposed on a free-carrier (Drude) response in combination with several symmetric Lorentz oscillators that describe the midinfrared response. Because the iron telluride compounds are multiband materials [34], the minimal description of the dielectric function usually consists of at least two Drude components [35],

$$\tilde{\epsilon}(\omega) = \epsilon_\infty - \sum_{j=1}^{2}\frac{\omega_{p,D;j}^2}{\omega^2 + i\omega/\tau_{D,j}}, \tag{6}$$

where ϵ_∞ has been previously defined, $\omega_{p,D;j}^2 = 4\pi n_j e^2/m_j^*$ and $1/\tau_{D,j}$ are the square of the plasma frequency and scattering rate for the delocalized (Drude) carriers, respectively, in the jth band, and n_j and m_j^* are the carrier concentration and effective mass. The values for $\omega_{p,D;j}$ and $1/\tau_{D,j}$ and the midinfrared oscillators are initially fit to the complex conductivity up to at least 1 eV using a nonlinear least-squares technique. Fits to the infrared-active mode encompass only a

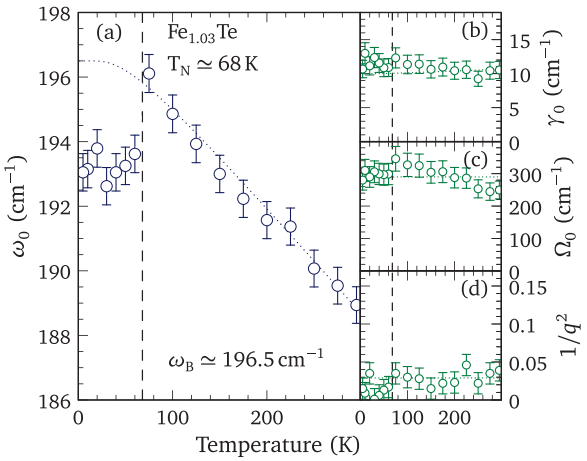

FIG. 2. The temperature dependence of the (a) infrared-active mode compared with the anharmonic decay model (dotted line), (b) linewidth and predicted dependence (dotted line), (c) oscillator strength, and (d) asymmetry parameter in $Fe_{1.03}Te$ ($T_N \simeq 68$ K); the dotted lines in the last two panels are drawn as a guide to the eye.

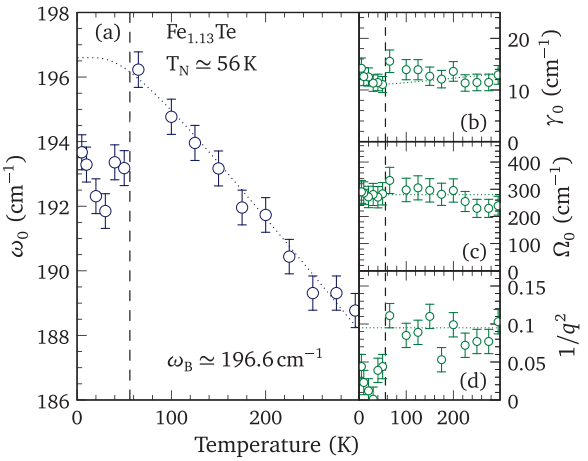

FIG. 3. The temperature dependence of the (a) infrared-active mode compared with the anharmonic decay model (dotted line), (b) linewidth and predicted dependence (dotted line), (c) oscillator strength, and (d) asymmetry parameter in $Fe_{1.13}Te$ ($T_N \simeq 56$ K); the dotted lines in the last two panels are drawn as a guide to the eye.

narrow region around the mode (typically ± 50 cm^{-1}), and as a result in addition to the vibrational parameters, only the Drude components and the width and strength of the lowest midinfrared oscillator are allowed to vary, while the other parameters remain fixed. The temperature dependence of $\omega_{p,D;1}$ and $1/\tau_{D,j}$ and the midinfrared oscillators in these materials have been previously discussed [19,21]. As Figs. 1(b) and 1(c) illustrate, both the background and the line shape are reproduced quite well using this approach.

The temperature dependence of ω_0, γ_0, Ω_0, and the asymmetry parameter $1/q^2$ of the infrared-active mode in $Fe_{1.03}Te$ is shown in Fig. 2. The frequency of the mode increases (hardens) in an almost linear fashion with decreasing temperature. At T_N there is an anomalous decrease (softening) in the frequency of the mode followed by a very weak temperature dependence; there is no evidence for a new infrared active B_u mode appearing below T_N. This is similar to the temperature dependence of the frequency of the B_{1g} mode in these materials [26–28]. The width of this mode shows very little temperature dependence either above or below T_N. While the strength of this mode may increase slightly as the temperature is lowered to T_N, it is also possible that, within error, it is constant; below T_N there is very little change. Above T_N, the asymmetry parameter $1/q^2 \simeq 0.03$, suggesting weak spin- or electron-phonon coupling [2]. Below T_N the asymmetry parameter $1/q^2$ decreases, and the line shape becomes almost perfectly symmetric; this inferred reduction in the phonon coupling may be related to the fact that in the AFM state the spin fluctuations are observed to decrease [36] and most signs of correlations disappear [37].

The temperature dependence of the infrared-active mode in $Fe_{1.13}Te$ has been fit using the procedure described above, and the results are shown in Fig. 3 (the temperature dependence of the optical conductivity and the fit at 30 K are shown in Fig. S1 in the Supplemental Material [38]). The behaviors of ω_0, γ_0, and Ω_0 are quite similar to those of $Fe_{1.03}Te$, although there does tend to be a bit more scatter in the data points. However, above T_N the asymmetry parameter $1/q^2 \simeq 0.1$, suggesting that the spin- or electron-phonon coupling is stronger in this material; as in $Fe_{1.03}Te$, below T_N the asymmetry parameter $1/q^2$ decreases, suggesting a decrease in correlations and a commensurate reduction in the coupling of the phonons to either the spin or charge.

Above T_N the behavior of ω_0 can be described quite well assuming a symmetric anharmonic decay into two acoustic modes with identical frequencies and opposite momenta [39,40]. A slightly modified functional form is employed here,

$$\omega_0(T) = \omega_B\left[1 - \frac{2C}{e^x - 1}\right], \tag{7}$$

$$\gamma_0(T) = \Gamma_0\left[1 + \frac{2\Gamma}{e^x - 1}\right], \tag{8}$$

where ω_B is the bare phonon frequency, Γ_0 is a residual linewidth, C and Γ are constants, and $x = \hbar\omega_B/(2k_BT)$; an advantage of this form is that the bare phonon frequency (residual linewidth) is recovered in the $T \to 0$ limit. The model fits to the $T > T_N$ data are indicated by the dotted lines in Figs. 2 and 3, yielding nearly identical values of $\omega_B \simeq 196.5$ and 196.6 cm^{-1} for $Fe_{1.03}Te$ and $Fe_{1.13}Te$, respectively.

The behavior of the infrared-active mode at T_N is also reminiscent of the E_u mode in $BaFe_2As_2$, which also experiences an anomalous softening below the magnetic and structural transition at $T_N \simeq 138$ K [41]; however, in that material the oscillator strength nearly doubles below T_N, whereas in $Fe_{1+\delta}Te$ it remains more or less unchanged.

2. *Lattice dynamics*

The frequencies and atomic intensities (squares of the vibrational amplitude of each atom that sum to unity) for the zone-center phonons have been calculated from first principles using the so-called frozen-phonon method, the details of which are described the Appendix. The results for the high-temperature tetragonal phase using the relaxed (experimental) unit-cell parameters (Table II in the Appendix) are shown in

TABLE I. Calculated frequencies and Fe atomic intensities in the high- (HT) and low-temperature (LT) phases of FeTe for the zone-center modes. For each phase, the results based on the relaxed and experimental (shown in parentheses) unit-cell parameters are considered; for the low-temperature phase, non-spin-polarized (NSP) and spin-polarized (SP) calculations are performed. All units are in cm^{-1} unless otherwise indicated.

$P4/nmm$ (HT)		Atomic intensity	$P2_1/m$ (LT)		Atomic intensity		Atomic intensity	
Symmetry	Theory	Fe	Symmetry	Theory NSP	Fe	Theory SP	Fe	Expt.[a]
E_g	98 (77)	0.11 (0.12)	A_g	98 (57)	0.10 (0.17)	84 (81)	0.13 (0.11)	
			B_g	99 (72)	0.10 (0.13)	85 (79)	0.13 (0.08)	
A_{1g}	170 (141)	0.00 (0.00)	A_g	173 (137)	0.00 (0.00)	145 (139)	0.15 (0.00)	160
E_u	249 (203)	0.70 (0.70)	B_u	245 (203)	0.70 (0.70)	241 (195)	0.70 (0.70)	196
			B_u	300 (254)	0.70 (0.70)	306 (267)	0.70 (0.70)	
B_{1g}	272 (221)	1.00 (1.00)	A_g	270 (210)	1.00 (0.89)	167	0.85	203
E_g	292 (223)	0.89 (0.88)	A_g	289 (226)	0.90 (0.92)	287 (243)	0.87 (0.89)	
			B_g	292 (215)	0.90 (0.87)	288 (245)	0.87 (0.92)	
A_{2u}	304 (257)	0.70 (0.69)	A_u	248 (196)	0.70 (0.70)	244 (189)	0.70 (0.70)	

[a]The Raman results are taken from Ref. [27]; infrared is from this work.

Table I and compared with experimental results; these results are in good agreement with other calculations [24,25]. It has been remarked that in this material the frequencies calculated using the experimental unit-cell parameters are in better agreement with the experimentally observed frequencies than the values determined from a relaxed unit cell [24], and that is indeed the case here. In the relaxed unit cell the Fe-Te bond is shorter, which has the effect of scaling up all of the frequencies by 20%–30%; however, we note that the character of the atomic intensities is essentially unaffected. The A_{1g} and B_{1g} Raman modes are calculated using the relaxed (experimental) unit-cell parameters at 170 (141) and 272 (221) cm^{-1}, respectively, and are pure Te and Fe vibrations, whereas the E_u mode is a mixture of the two. Using the experimental unit cell, the calculated frequency for the E_u mode of 203 cm^{-1} is quite close to the measured value of $\simeq$196 cm^{-1}, as are the values for the A_{1g} and B_{1g} modes [27].

The frequencies and atomic intensities for the low-temperature monoclinic phase have also been calculated using the relaxed (experimental) unit-cell parameters (Table III in the Appendix), and the results are listed in Table I. As previously noted, the lower symmetry results in the splitting of the doubly degenerate $E_g \rightarrow A_g + B_g$ and $E_u \rightarrow 2B_u$ modes. In the nonmagnetic calculation (non spin polarized), the calculated frequencies for the relaxed and experimental unit cells match quite well with their counterparts in the tetragonal phase, and the character of the modes does not change substantially. In the relaxed unit cell the splitting of the upper and lower E_g modes is negligible ($\simeq$2 cm^{-1}); however, in the experimental unit cell this splitting is much larger, $\simeq$20 cm^{-1}. In both the experimental and relaxed geometries, the E_u mode is predicted to split by $\simeq$50 cm^{-1}. A simple empirical force-constant model [42] reproduces the size of the splitting below T_N and indicates that the two B_u modes should have roughly the same strength. Using a splitting of $\simeq$50 cm^{-1}, a new mode might be expected at $\simeq$240 cm^{-1}; however, there does not appear to be any experimental evidence for a new mode below T_N [Fig. 1(a) and Fig. S1(a) in the Supplementary Material].

The non-spin-polarized calculation does not take into consideration the antiferromagnetic ground state of this material [4]. Accordingly, the spins on the two Fe sites have been placed in an antiferromagnetic configuration, while the Te atoms remain nonmagnetic; the frequencies and atomic characters are then calculated for a spin-polarized case using both the relaxed and experimentally determined unit-cell parameters, and the results are listed in Table I. The introduction of magnetic order has a significant effect on some modes, changing both the frequency and the character of the vibration; however, we note that the E_u, upper E_g, and A_{2u} modes experience only a small effect. The small predicted downward shift in the lower B_u mode of $\simeq$4–7 cm^{-1} for the spin-polarized case is in good agreement with the experimentally observed softening of this mode of between 2 and 4 cm^{-1} in $Fe_{1+\delta}Te$ below T_N.

B. $FeTe_{0.55}Se_{0.45}$

The real part of the optical conductivity of superconducting $FeTe_{0.55}Se_{0.45}$ in the region of the infrared-active phonon at $\simeq$213 cm^{-1} is shown in Fig. 4(a) [21]. The substitution of Se for Te in this material has the effect of shifting the frequency of the E_u mode up about 10%. The temperature dependence of the E_u mode has been fit to the complex conductivity using the asymmetric Fano line shape in Eq. (4) superimposed on a Drude-Lorentz background; as Figs. 4(b) and 4(c) illustrate, both the background and the line shape are reproduced quite well. In several cases, it appears as though there is a weak sideband at $\simeq$240 cm^{-1}; however, no new mode is predicted in this material, suggesting that such features are the result of an asymmetric line shape.

The temperature dependence of the frequency and linewidth of the mode, shown in Figs. 5(a) and 5(b), respectively, agrees quite well with the anharmonic decay model. The strength of the mode shown in Fig. 5(c) may be increasing somewhat with decreasing temperature, but within the accuracy of the fits it is also possible that it is temperature independent. The asymmetry parameter is small at room temperature, $1/q^2 \simeq 0.05$, but increases with temperature, reaching a maximum of $1/q^2 \simeq 0.13$ at $\simeq$125 K before decreasing at low temperature, as shown in Fig. 5(d). This would tend to indicate that the spin- or electron-phonon coupling of the E_u mode is becoming significant, and indeed it is considerably larger than what is observed in related iron pnictide materials [2]. The decrease in

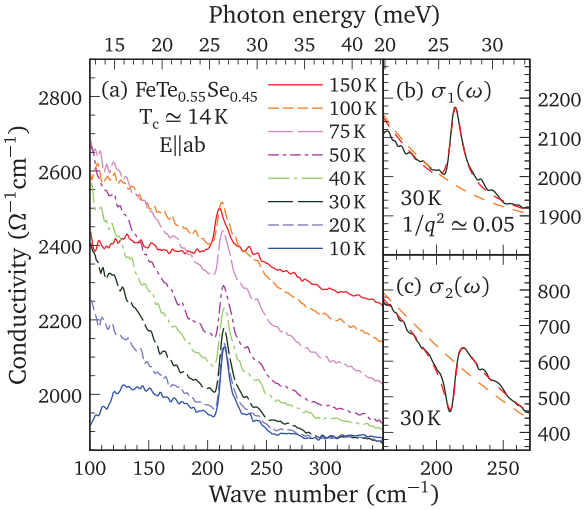

FIG. 4. (a) The real part of the optical conductivity of $FeTe_{0.55}Se_{0.45}$ above and below $T_c \simeq 14$ K in the region of the infrared-active E_u mode at $\simeq$213 cm^{-1}. (b) Fano oscillator fit (short-dashed line) to $\sigma_1(\omega)$ at 30 K with the Drude-Lorentz background (long-dashed line) and (c) the simultaneous fit to $\sigma_2(\omega)$.

$1/q^2$ at low temperature is correlated with the rapid decrease in the Hall coefficient below 100 K [43], suggesting that the electron-phonon coupling is related to a specific carrier pocket in this material. While electron-phonon coupling is present in this material at low temperatures, it is thought that the electron-phonon coupling constant λ in this material is quite small ($\lambda \simeq 0.01$) [44]. The low values for λ do not support the high T_c's observed in iron-based superconductors, implying that these materials are not phonon-mediated superconductors [45]. However, a detailed analysis of the five-orbital Hubbard-Holstein model for iron pnictides has demonstrated that a relatively small electron-phonon interaction arising from the Fe-ion oscillation can induce substantial d-orbital fluctuations [46,47], as well as the anion electronic polarization [48]. These orbital fluctuations give rise to a strong pairing interaction and mediate an s_{++} superconducting state. In addition, a large Fe isotope effect has been reported in $SmFeAsO_{1-x}Fe_x$ and $Ba_{1-x}K_xFe_2As_2$ [49], indicating that electron-phonon coupling likely plays some role in the pairing mechanism. Our experimental results in the $Fe_{1+y}Te_{1-x}Se_x$ system, in combination with the above theoretical and experimental studies, suggest that electron-phonon coupling may be a necessary prerequisite for superconductivity in this class of materials.

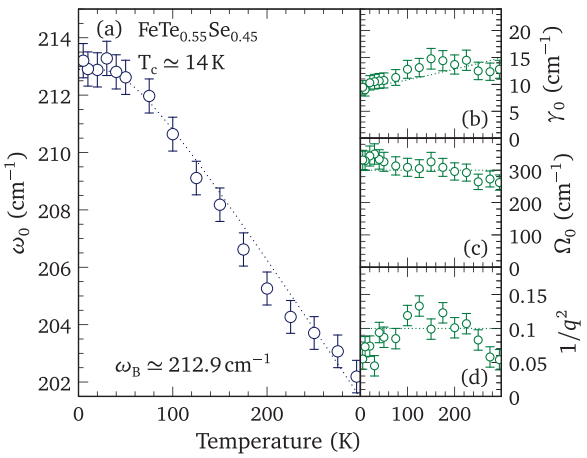

FIG. 5. The temperature dependence of the (a) infrared-active E_u mode compared with the anharmonic decay model (dotted line), (b) linewidth and predicted dependence (dotted line), (c) oscillator strength, and (d) asymmetry parameter in $FeTe_{0.55}Se_{0.45}$ ($T_c = 14$ K); the dotted lines in the last two panels are drawn as a guide to the eye.

IV. CONCLUSIONS

The detailed temperature dependence of the infrared-active mode has been fit in $Fe_{1.03}Te$ and $Fe_{1.13}Te$ using an asymmetric Fano line shape superimposed on a background of Drude free carriers and symmetric Lorentz oscillators. In both materials, above T_N the frequency increases as the temperature is lowered; this behavior is described quite well by an anharmonic decay process. Below T_N, there is an abrupt softening of this mode in both materials, below which it displays little temperature dependence. While the frequency of the mode and the size of the shift below T_N are predicted reasonably well from first-principles calculations (with some caveats), the predicted splitting of the infrared-active mode is not observed. In both materials, the phonon has a slightly asymmetric line shape above T_N, suggesting that there is coupling of the phonons to either spin or charge; however, $1/q^2$ decreases and the profile becomes more symmetric below T_N, suggesting this coupling is reduced. The E_u mode in superconducting $FeTe_{0.55}Se_{0.45}$ has been fit in a similar fashion and displays an asymmetry at all temperatures, which is most pronounced between 100 and 200 K. The temperature dependence of this mode is once again described quite well by an anharmonic decay process over the entire temperature range. The asymmetric nature of the E_u mode is an indication of spin- or electron-phonon coupling, which may be a necessary prerequisite for superconductivity in iron-based materials.

ACKNOWLEDGMENTS

We would like to acknowledge helpful discussions with T. Birol. We are indebted to S. V. Dordevic for referring us to a phenomenological Fano line shape, developed by A. Damascelli and A. Kuzmenko. This work is supported by the Office of Science, US Department of Energy under Contract No. DE-SC0012704. J.S. and R.D.Z. are supported by the Center for Emergent Superconductivity, an Energy Frontier Research Center funded by the US Department of Energy, Office of Science.

APPENDIX: LATTICE DYNAMICS

1. $P4/nmm$ (high temperature)

The total energy of FeTe was calculated with the generalized gradient approximation (GGA) using the full-potential linearized augmented plane-wave (FP-LAPW) method [50] with local-orbital extensions [51] in the WIEN2K implementation [52]. An examination of different Monkhorst-Pack k-point meshes indicated that 175 k points ($6 \times 6 \times 4$ mesh) and

TABLE II. The experimental and theoretical lattice constants and atomic fractional coordinates for the relaxed structure of FeTe for the high-temperature tetragonal $P4/nmm$ space group. The fractional coordinate for the Fe atom is $(\frac{3}{4}\frac{1}{4}0)$. The Fe-Te bond lengths are also shown, while the Fe-Fe and Te-Te bond lengths, 2.6960 and 2.8126 Å, respectively, are essentially identical for the two structures.

	Experiment[a]	GGA
a (Å)	3.8127	3.8126
c (Å)	6.2450	6.2448
Te$(\frac{1}{4}\frac{1}{4}z)$	0.2813	0.2569
Fe-Te (Å)	2.5923	2.4915

[a]Reference [4] [Supplemental Material, Table I, Sec. (a)].

$R_{mt}k_{\max} = 7.5$ was sufficient for good energy convergence. The geometry of the unit cell was refined through an iterative process whereby the volume was optimized with respect to the total energy while the c/a ratio remained fixed. The atomic fractional coordinates were then relaxed with respect to the total force, typically resulting in residual forces of less than 1 mRy/a.u. This procedure was repeated until no further improvement was obtained. A comparison of the experimental and calculated (relaxed) unit-cell parameters is shown in Table II. Note that while the unit-cell parameters are nearly identical to the experimentally determined values, the position of the Te atom has shifted somewhat.

The phonons were determined using the direct method. To determine the phonons at the zone center, a $1 \times 1 \times 1$ supercell is sufficient. To obtain a complete set of Hellmann-Feynman forces, a total of four independent displacements is required; because there are always some residual forces at the atomic sites we considered symmetric displacements, which doubles this number, resulting in a total of eight atomic displacements. In this case, displacement amplitudes of 0.03 Å were used. The calculations converged when the successive changes for the forces on each atom were less than 0.1 mRy/a.u. The residual forces were collected for each set of symmetric displacements, and a list of the Hellmann-Feynman forces was generated. Using the program PHONON [53], the cumulative force constants deconvoluted from the Hellmann-Feynman forces were introduced into the dynamical matrix, which was then diagonalized in order to obtain the phonon frequencies; the atomic intensities were further calculated to describe the character of the vibration. The results are shown in Table I.

2. $P2_1/m$ (low temperature)

The procedure that was used to calculate the geometry of the room-temperature tetragonal phase was repeated for the low-temperature monoclinic phase; the same k point mesh and $R_{mt}k_{\max}$ were used. The optimized unit-cell parameters are compared with the experimental values and shown in Table III. Once again, the calculated unit-cell parameters are nearly identical to the experimental values; however, the Fe and Te atoms have undergone small shifts, resulting in a decrease of the Fe-Te bond lengths. Interestingly, the Fe-Fe bond modulation observed experimentally is not captured in the non-spin-polarized GGA result in which the Fe-Fe bonds are almost identical. To calculate the zone-center phonons, a $1 \times 1 \times 1$ supercell was employed. In the monoclinic phase a total of six independent displacements are required; symmetric displacements double this number to 12. Displacement amplitudes of 0.03 Å were used.

Two different cases were considered for this symmetry. In the first case the system was assumed to be nonmagnetic, the spins on the Fe and Te sites were ignored, and a non-spin-polarized (NSP) calculation was performed. The calculated phonon frequencies and atomic intensities are listed in Table I. In the second case the spins on the Fe sites were specified to be in an antiferromagnetic configuration, the Te atoms were assumed to be nonmagnetic, and a spin-polarized calculation was performed. If the fractional coordinates are relaxed in this case, the position of the Te atom is closer to the experimental value, and a Fe-Fe bond modulation is observed (Table III). However, given that this structure appears to be intermediate between the non-spin-polarized and the experimental unit-cell parameters, we did not perform a phonon calculation. Using the previously established criteria for convergence, we found the magnetic moments are about $1.7\mu_B$/Fe for the (non-spin-polarized) relaxed unit cell, which is very close to the expected value of $2\mu_B$/Fe observed in other work [54]. When the experimental unit cell was used, the magnetic moments increased to $2.2\mu_B$/Fe; however, this results in a calculated frequency of less than zero for one of the A_g modes, and this unphysical value indicates that within the scope of this calculation the structure is unstable.

TABLE III. The experimental and theoretical lattice constants and atomic fractional coordinates for the relaxed structure of FeTe for the low-temperature monoclinic $P2_1/m$ space group. The Fe-Fe and Fe-Te bond lengths are also shown.

	Experiment[a]		GGA (NSP)		GGA (SP)	
a (Å)	3.8346		3.8391		3.8391	
b (Å)	3.7836		3.7897		3.7897	
c (Å)	6.2567		6.2649		6.2649	
β (°)	89.21		89.24		89.24	
Fe$(x\ \frac{1}{4}\ z)$	0.7612	0.0033	0.7501	0.0013	0.7507	0.0011
Te$(x\ \frac{1}{4}\ z)$	0.2586	0.2822	0.2448	0.2559	0.2454	0.2717
Fe-Fe (Å)	2.633/2.756		2.697/2.698		2.693/2.701	
Fe-Te (Å)	2.582/2.603/2.604		2.487/2.495/2.496		2.552/2.559/2.562	

[a]Reference [8].

[1] D. C. Johnston, The puzzle of high temperature superconductivity in layered iron pnictides and chalcogenides, Adv. Phys. **59**, 803 (2010).

[2] B. Xu, Y. M. Dai, B. Shen, H. Xiao, Z. R. Ye, A. Forget, D. Colson, D. L. Feng, H. H. Wen, C. C. Homes, X. G. Qiu, and R. P. S. M. Lobo, Anomalous phonon redshift in K-doped $BaFe_2As_2$ iron pnictides, Phys. Rev. B **91**, 104510 (2015).

[3] Z. P. Yin, K. Haule, and G. Kotliar, Kinetic frustration and the nature of the magnetic and paramagnetic states in iron pnictides and iron chalcogenides, Nat. Mater. **10**, 932 (2011).

[4] W. Bao, Y. Qiu, Q. Huang, M. A. Green, P. Zajdel, M. R. Fitzsimmons, M. Zhernenkov, S. Chang, M. Fang, B. Qian, E. K. Vehstedt, J. Yang, H. M. Pham, L. Spinu, and Z. Q. Mao, Tunable $(\delta\pi, \delta\pi)$-Type Antiferromagnetic Order in α-Fe(Te,Se) Superconductors, Phys. Rev. Lett. **102**, 247001 (2009).

[5] M. J. Han and S. Y. Savrasov, Doping Driven $(\pi,0)$ Nesting and Magnetic Properties of $Fe_{1+x}Te$ Superconductors, Phys. Rev. Lett. **103**, 067001 (2009).

[6] A. Martinelli, A. Palenzona, M. Tropeano, C. Ferdeghini, M. Putti, M. R. Cimberle, T. D. Nguyen, M. Affronte, and C. Ritter, From antiferromagnetism to superconductivity in $Fe_{1+y}Te_{1-x}Se_x (0 \leqslant x \leqslant 0.20)$: Neutron powder diffraction analysis, Phys. Rev. B **81**, 094115 (2010).

[7] I. A. Zaliznyak, Z. Xu, J. M. Tranquada, G. Gu, A. M. Tsvelik, and M. B. Stone, Unconventional Temperature Enhanced Magnetism in $Fe_{1.1}$ Te, Phys. Rev. Lett. **107**, 216403 (2011).

[8] I. A. Zaliznyak, Z. J. Xu, J. S. Wen, J. M. Tranquada, G. D. Gu, V. Solovyov, V. N. Glazkov, A. I. Zheludev, V. O. Garlea, and M. B. Stone, Continuous magnetic and structural phase transitions in $Fe_{1+y}Te$, Phys. Rev. B **85**, 085105 (2012).

[9] D. Fobes, I. A. Zaliznyak, Z. Xu, R. Zhong, G. Gu, J. M. Tranquada, L. Harriger, D. Singh, V. O. Garlea, M. Lumsden, and B. Winn, Ferro-Orbital Ordering Transition in Iron Telluride Fe_{1+y} Te, Phys. Rev. Lett. **112**, 187202 (2014).

[10] X. Liu, C.-C. Lee, Z. J. Xu, J. S. Wen, G. Gu, W. Ku, J. M. Tranquada, and J. P. Hill, X-ray diffuse scattering study of local distortions in $Fe_{1-x}Te$ induced by excess Fe, Phys. Rev. B **83**, 184523 (2011).

[11] E. E. Rodriguez, C. Stock, P. Zajdel, K. L. Krycka, C. F. Majkrzak, P. Zavalij, and M. A. Green, Magnetic-crystallographic phase diagram of the superconducting parent compound $Fe_{1+x}Te$, Phys. Rev. B **84**, 064403 (2011).

[12] S. Li, C. de la Cruz, Q. Huang, Y. Chen, J. W. Lynn, J. Hu, Y.-L. Huang, F.-C. Hsu, K.-W. Yeh, M.-K. Wu, and P. Dai, First-order magnetic and structural phase transitions in $Fe_{1+y}Se_xTe_{1-x}$, Phys. Rev. B **79**, 054503 (2009).

[13] T. J. Liu, J. Hu, B. Qian, D. Fobes, Z. Q. Mao, W. Bao, M. Reehuis, S. A. J. Kimber, K. Prokeš, S. Matas, D. N. Argyriou, A. Hiess, A. Rotaru, H. Pham, L. Spinu, Y. Qiu, V. Thampy, A. T. Savici, J. A. Rodriguez, and C. Broholm, From $(\pi,0)$ magnetic order to superconductivity with (π,π) magnetic resonance in $Fe_{1.02}$ Te_{1-x} Se_x, Nat. Mater. **9**, 718 (2010).

[14] M. H. Fang, H. M. Pham, B. Qian, T. J. Liu, E. K. Vehstedt, Y. Liu, L. Spinu, and Z. Q. Mao, Superconductivity close to magnetic instability in $Fe(Se_{1-x}Te_x)_{0.82}$, Phys. Rev. B **78**, 224503 (2008).

[15] T. Taen, Y. Tsuchiya, Y. Nakajima, and T. Tamegai, Superconductivity at $T_c \sim 14$ K in single-crystalline $FeTe_{0.61}Se_{0.39}$, Phys. Rev. B **80**, 092502 (2009).

[16] B. C. Sales, A. S. Sefat, M. A. McGuire, R. Y. Jin, D. Mandrus, and Y. Mozharivskyj, Bulk superconductivity at 14 K in single crystals of $Fe_{1+y}Te_xSe_{1-x}$, Phys. Rev. B **79**, 094521 (2009).

[17] G. F. Chen, Z. G. Chen, J. Dong, W. Z. Hu, G. Li, X. D. Zhang, P. Zheng, J. L. Luo, and N. L. Wang, Electronic properties of single-crystalline $Fe_{1.05}Te$ and $Fe_{1.03}Se_{0.30}Te_{0.70}$, Phys. Rev. B **79**, 140509(R) (2009).

[18] J. N. Hancock, S. I. Mirzaei, J. Gillett, S. E. Sebastian, J. Teyssier, R. Viennois, E. Giannini, and D. van der Marel, Strong coupling to magnetic fluctuations in the charge dynamics of iron-based superconductors, Phys. Rev. B **82**, 014523 (2010).

[19] Y. M. Dai, A. Akrap, J. Schneeloch, R. D. Zhong, T. S. Liu, G. D. Gu, Q. Li, and C. C. Homes, Spectral weight transfer in strongly correlated $Fe_{1.03}$ Te, Phys. Rev. B **90**, 121114 (2014).

[20] C. C. Homes, A. Akrap, J. S. Wen, Z. J. Xu, Z. W. Lin, Q. Li, and G. D. Gu, Electronic correlations and unusual superconducting response in the optical properties of the iron chalcogenide $FeTe_{0.55}$ $Se_{0.45}$, Phys. Rev. B **81**, 180508 (2010).

[21] C. C. Homes, Y. M. Dai, J. S. Wen, Z. J. Xu, and G. D. Gu, $FeTe_{0.55}$ $Se_{0.45}$: A multiband superconductor in the clean and dirty limit, Phys. Rev. B **91**, 144503 (2015).

[22] A. Pimenov, S. Engelbrecht, A. M. Shuvaev, B. B. Jin, P. H. Wu, B. Xu, L. X. Cao, and E. Schachinger, Terahertz conductivity in $FeSe_{0.5}$ $Te_{0.5}$ superconducting films, New J. Phys. **15**, 013032 (2013).

[23] A. Perucchi, B. Joseph, S. Caramazza, M. Autore, E. Bellingeri, S. Kawale, C. Ferdeghini, M. Putti, S. Lupi, and P. Dore, Two-band conductivity of a $FeSe_{0.5}$ $Te_{0.5}$ film by reflectance measurements in the terahertz and infrared range, Supercond. Sci. Technol. **27**, 125011 (2014).

[24] T.-L. Xia, D. Hou, S. C. Zhao, A. M. Zhang, G. F. Chen, J. L. Luo, N. L. Wang, J. H. Wei, Z.-Y. Lu, and Q. M. Zhang, Raman phonons of α-FeTe and $Fe_{1.03}Se_{0.3}Te_{0.7}$ single crystals, Phys. Rev. B **79**, 140510(R) (2009).

[25] K. Okazaki, S. Sugai, S. Niitaka, and H. Takagi, Phonon, two-magnon, and electronic Raman scattering of $Fe_{1+y}Te_{1-x}Se_x$, Phys. Rev. B **83**, 035103 (2011).

[26] V. Gnezdilov, Yu. Pashkevich, P. Lemmens, A. Gusev, K. Lamonova, T. Shevtsova, I. Vitebskiy, O. Afanasiev, S. Gnatchenko, V. Tsurkan, J. Deisenhofer, and A. Loidl, Anomalous optical phonons in FeTe chalcogenides: Spin state, magnetic order, and lattice anharmonicity, Phys. Rev. B **83**, 245127 (2011).

[27] Y. J. Um, A. Subedi, P. Toulemonde, A. Y. Ganin, L. Boeri, M. Rahlenbeck, Y. Liu, C. T. Lin, S. J. E. Carlsson, A. Sulpice, M. J. Rosseinsky, B. Keimer, and M. Le Tacon, Anomalous dependence of c-axis polarized Fe B_{1g} phonon mode with Fe and Se concentrations in $Fe_{1+y}Te_{1-x}Se_x$, Phys. Rev. B **85**, 064519 (2012).

[28] Z. V. Popović, N. Lazarević, S. Bogdanović, M. M. Radonjić, D. Tanasković, R. Hu, H. Lei, and C. Petrovic, Signatures of the spin-phonon coupling in alloys, Solid State Commun. **193**, 51 (2014).

[29] C. C. Homes, M. Reedyk, D. A. Cradles, and T. Timusk, Technique for measuring the reflectance of irregular, submillimeter-sized samples, Appl. Opt. **32**, 2976 (1993).

[30] M. Dressel and G. Grüner, *Electrodynamics of Solids* (Cambridge University Press, Cambridge, 2001).

[31] U. Fano, Effects of configuration interaction on intensities and phase shifts, Phys. Rev. **124**, 1866 (1961).

[32] A. Damascelli, Optical spectroscopy of quantum spin systems, Ph.D. thesis, University of Groningen, 1996, p. 21.

[33] A. Kuzmenko, REFFIT software, 2014, http://optics.unige.ch/alexey/reffit.html.

[34] A. Subedi, L. Zhang, D. J. Singh, and M. H. Du, Density functional study of FeS, FeSe, and FeTe: Electronic structure, magnetism, phonons, and superconductivity, Phys. Rev. B **78**, 134514 (2008).

[35] D. Wu, N. Barišić, P. Kallina, A. Faridian, B. Gorshunov, N. Drichko, L. J. Li, X. Lin, G. H. Cao, Z. A. Xu, N. L. Wang, and M. Dressel, Optical investigations of the normal and superconducting states reveal two electronic subsystems in iron pnictides, Phys. Rev. B **81**, 100512(R) (2010).

[36] Y. Zhang, F. Chen, C. He, L. X. Yang, B. P. Xie, Y. L. Xie, X. H. Chen, M. Fang, M. Arita, K. Shimada, H. Namatame, M. Taniguchi, J. P. Hu, and D. L. Feng, Strong correlations and spin-density-wave phase induced by a massive spectral weight redistribution in α -$Fe_{1.06}$Te, Phys. Rev. B **82**, 165113 (2010).

[37] P.-H. Lin, Y. Texier, A. Taleb-Ibrahimi, P. Le Fèvre, F. Bertran, E. Giannini, M. Grioni, and V. Brouet, Nature of the Bad Metallic Behavior of $Fe_{1.06}$ Te Inferred from its Evolution in the Magnetic State, Phys. Rev. Lett. **111**, 217002 (2013).

[38] See Supplemental Material at http://link.aps.org/supplemental/10.1103/PhysRevB.93.125135 for temperature dependence of the optical conductivity of $Fe_{1.13}$Te in the region of the infrared-active mode.

[39] P. G. Klemens, Anharmonic decay of optical phonons, Phys. Rev. **148**, 845 (1966).

[40] J. Menéndez and M. Cardona, Temperature dependence of the first-order Raman scattering by phonons in Si, Ge, and α-Sn: Anharmonic effects, Phys. Rev. B **29**, 2051 (1984).

[41] A. Akrap, J. J. Tu, L. J. Li, G. H. Cao, Z. A. Xu, and C. C. Homes, Infrared phonon anomaly in $BaFe_2As_2$, Phys. Rev. B **80**, 180502 (2009).

[42] E. Dowty, VIBRATZ software, Shape Software (Kingsport, TN, 2001).

[43] I. Tsukada, M. Hanawa, S. Komiya, T. Akiike, R. Tanaka, Y. Imai, and A. Maeda, Hall effect in superconducting $Fe(Se_{0.5}Te_{0.5})$ thin films, Phys. Rev. B **81**, 054515 (2010).

[44] C. W. Luo, I. H. Wu, P. C. Cheng, J.-Y. Lin, K. H. Wu, T. M. Uen, J. Y. Juang, T. Kobayashi, Y. C. Wen, T. W Huang, K. W. Yeh, M. K. Wu, D. A. Chareev, O. S. Volkova, and A. N. Vasiliev, Ultrafast dynamics and phonon softening in $Fe_{1+y}Se_{1-x}Te_x$ single crystals, New J. Phys. **14**, 103053 (2012).

[45] L. Boeri, O. V. Dolgov, and A. A. Golubov, Is $LaFeAsO_{1-x}F_x$ an Electron-Phonon Superconductor? Phys. Rev. Lett. **101**, 026403 (2008).

[46] H. Kontani and S. Onari, Orbital-Fluctuation-Mediated Superconductivity in Iron Pnictides: Analysis of the Five-Orbital Hubbard-Holstein Model, Phys. Rev. Lett. **104**, 157001 (2010).

[47] T. Saito, S. Onari, and H. Kontani, Orbital fluctuation theory in iron pnictides: Effects of As-Fe-As bond angle, isotope substitution, and Z^2-orbital pocket on superconductivity, Phys. Rev. B **82**, 144510 (2010).

[48] C. Ma, L. Wu, W.-G. Yin, H. Yang, H. Shi, Z. Wang, J. Li, C. C. Homes, and Y. Zhu, Strong Coupling of the Iron-Quadrupole and Anion-Dipole Polarizations in $Ba(Fe_{1-x}\ Co_x)_2\ As_2$, Phys. Rev. Lett. **112**, 077001 (2014).

[49] R. H. Liu, T. Wu, G. Wu, H. Chen, X. F. Wang, Y. L. Xie, J. J. Ying, Y. J. Yan, Q. J. Li, B. C. Shi, W. S. Chu, Z. Y. Wu, and X. H. Chen, A large iron isotope effect in $SmFeAsO_{1-x}\ F_x$ and $Ba_{1-x}\ K_x\ Fe_2\ As_2$ Nature **459**, 64 (2009).

[50] D. J. Singh, *Planewaves, Pseudopotentials and the LAPW method* (Kluwer Adademic, Boston, 1994).

[51] D. Singh, Ground-state properties of lanthanum: Treatment of extended-core states, Phys. Rev. B **43**, 6388 (1991).

[52] P. Blaha, K. Schwarz, G. K. H. Madsen, D. Kvasnicka, and J. Luitz, *WIEN2K, an Augmented Plane Wave Plus Local Orbitals Program for Calculating Crystal Properties* (Technische Universität Wien, Vienna, 2001).

[53] K. Parlinksi, PHONON software, 2003, http://www.computingformaterials.com/index.html.

[54] H. Gretarsson, A. Lupascu, J. Kim, D. Casa, T. Gog, W. Wu, S. R. Julian, Z. J. Xu, J. S. Wen, G. D. Gu, R. H. Yuan, Z. G. Chen, N.-L. Wang, S. Khim, K. H. Kim, M. Ishikado, I. Jarrige, S. Shamoto, J.-H. Chu, I. R. Fisher, and Y.-J. Kim, Revealing the dual nature of magnetism in iron pnictides and iron chalcogenides using x-ray emission spectroscopy, Phys. Rev. B **84**, 100509(R) (2011).